

Long-term multi-wavelength variations of *Fermi* blazar 3C 279

Bing-Kai Zhang^{1,2}, Min Jin¹, Xiao-Yun Zhao¹, Li Zhang³ and Ben-Zhong Dai³

¹ Department of Physics, Fuyang Normal University, Fuyang 236037, China; zhangbk_ynu@163.com

² Key Laboratory of Functional Materials and Devices for Informatics of Anhui Higher Education Institutes, Fuyang Normal University, Fuyang 236037, China

³ Department of Astronomy, Yunnan University, Kunming 650091, China

Received 2021 January 20; accepted 2021 March 10

Abstract Long-term optical, X-ray and γ -ray data of blazar 3C 279 have been compiled from *Swift*-XRT, *RXTE*-PCA, *Fermi*-LAT, SMARTS and literature. The source exhibits strong variability on long timescales. From the 1980s until now, the optical *R* band light curve spans more than 32 yr, and a possible 5.6-yr-long quasi-periodic variation component has been found in it. The optical spectral behavior has been investigated. In the optical band, the mean spectral index is -1.71 . The source exhibits an obvious special spectral behavior. In the low state, the source manifests a clear bluer-when-brighter behavior in the sense that the optical spectrum turns harder (flatter) when the brightness increases. While in the high state, the optical spectrum is stable, which means the source spectral index does not vary with brightness. The correlation analysis has been performed among optical, X-ray and γ -ray energy bands. The result indicates that the variations of γ -ray and X-ray bands are well correlated without time delay on the timescale of days, and their variations exhibit weak correlations with those of the optical band. The variations, especially outbursts, are simultaneous, but the magnitude of variations is disproportionate. The detailed analysis reveals that the main outbursts exhibit strong correlations in different γ -ray, X-ray and optical bands.

Key words: galaxies: active — BL Lacertae objects: general — quasars: general — quasars: individual (3C 279)

1 INTRODUCTION

Blazars, comprising BL Lacs and FSRQs, are the most extreme subclass of active galactic nuclei (AGNs) with a relativistic jet pointing along our line of sight (Urry & Padovani 1995). They radiate in all electromagnetic bands from radio to γ -rays, and exhibit non-thermal emission. In general, there are two typical broad peaks in their spectral energy distributions (SEDs). One is the low energy peak which lies between infrared and optical bands, even extending to X-ray band, and another is the high energy peak which is located from MeV to TeV γ -ray. The low energy peak can be interpreted by synchrotron radiation from relativistic energy electrons in the jet, while the mechanism of the second peak is an open question. At present, two typical models, leptonic model and hadronic scenario, are used to describe the high energy peak. Blazars exhibit violent variability from radio band to very high energy γ -ray band on diverse timescales which range from years to days, and even to several minutes. So, the study

of their variability is an important tool to provide valuable information about their nature.

3C 279, known as a flat spectrum radio quasar (FSRQ) with $z = 0.538$, is the first quasar which was discovered to exhibit apparent super-luminal motion (Whitney et al. 1971; Unwin et al. 1989). The apparent speeds can range up to $\beta_{\text{app}} \sim 17$ (Jorstad et al. 2004). 3C 279 is one of the first blazars which has been detected to emit γ -rays (Hartman et al. 1992). It is also the first FSRQ discovered to emit very high energy γ -rays (MAGIC Collaboration et al. 2008). Since 2008, 3C 279 has been observed continuously at high energy γ -rays ($E > 100$ MeV) by the *Fermi* satellite. The shortest doubling timescale of 1.19 hr has been reported in γ -ray variability during March-April 2014 (Paliya et al. 2015).

The variable behavior of 3C 279 has been widely studied in the optical band. It shows very large and rapid variations in brightness. A very large and violent optical outburst from $B = 18$ to 11.27 mag in ~ 1.5 yr was reported by Eachus & Liller (1975). After 1951, the source became

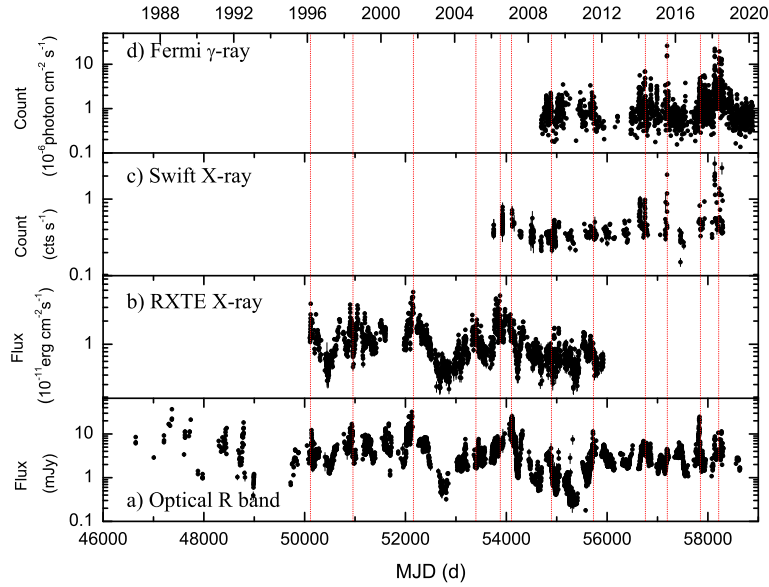


Fig. 1 The long-term different energy band light curves of blazar 3C 279. Panels (a) to (d) represent the light curves of optical (R band), *RXTE* X-ray (2–10 KeV), *Swift* X-ray (0.3–10 KeV) and *Fermi* γ -ray (0.1–300 GeV) energy bands, respectively. The vertical red dotted lines have been drawn near the main flares to guide the eyes. Calendar dates are along the top and MJDs are expressed at the bottom.

less active. Then, since 1987, the source exhibited more active variation. A rapid outburst of 2 mag within 24 hr was reported (Webb et al. 1990), and the most rapid optical V band variation by 1.17 mag in 40 min was observed on 1996 May 22 by Xie et al. (1999). During 2001–2002, the source exhibited optical R band variations up to 0.5 mag in 24 hr and variations up to 0.13 mag in 3 hr (Kartalpe & Balonek 2007). A strong flux decline ($\Delta R > 1.1$ mag in 13 d) was reported according to the Whole Earth Blazar Telescope (WEBT) campaign during 2005–2006 (Böttcher et al. 2007). With infrared K -band data, a strong period of 7.1 ± 0.44 yr was reported by Fan (1999). In the optical R light curve, there seemed to be a 256-d quasi-periodic signal (Sandrinelli et al. 2016).

The source 3C 279 has been intensively studied through several simultaneous multi-wavelength campaigns (Hartman et al. 1996; Wehrle et al. 1998; Böttcher et al. 2007; Shah et al. 2019; Larionov et al. 2020; Prince 2020), and the correlation between the variations of different energy bands has been investigated. For example, a clear radio-optical correlation with 0–35 d time lag was identified by Tornikoski et al. (1994) and Zhang et al. (2017). Between optical and near-infrared bands, the correlation was seen historically in 3C 279 (Hartman et al. 1996; Wehrle et al. 1998). Between infrared and gamma-rays, Bonning et al. (2012) found weak correlations. Hartman et al. (2001) investigated cross-correlations among optical, X-ray and γ -ray bands, and ascertained no consistent tendencies although a significant optical/ γ -ray correlation was found during 1999, with an ~ 2.5 -d γ -ray lag. Chatterjee et al.

(2008) asserted that variations were significantly correlated between radio, optical and X-ray bands. Utilizing the first two-year *Fermi* data, Hayashida et al. (2012) ascertained γ -ray emission preceded that in optical by about 10 d. However, they found a lack of correlation between variations in X-ray and γ -ray bands during 2008–2010. They also detected an X-ray flare with no obvious counterpart in other energy bands. On the contrary, the different trends in May and June 2011 reported by Aleksić et al. (2014) implied that X-rays were correlated with γ -rays whereas the optical band seemed to have no significant correlation with γ -rays. With decade-long (2008–2018) data, Larionov et al. (2020) also concluded that the X-rays were correlated well with γ -rays with no lag being greater than 3 hr, and the γ -ray flux presented a complex relationship with optical flux, changing with the state of the source activity. During the flare of 2017–2018, 3C 279 displayed an obvious correlation between γ -rays and X-rays with no delay (Prince 2020).

With the accumulation of observed data from 3C 279, it is very meaningful to research the long-term multi-band variability behavior of this source. The outline of the paper is arranged as follows. The second section describes the light curves of optical, X-ray and γ -ray bands of 3C 279. Then in the third section, we search for quasi-periodic variable signals in the optical light curve. After this, we analyze the optical spectral behavior in the fourth section, and investigate cross correlations between three different energy bands in the fifth section. Finally we give a discussion and summarize our findings in the sixth section.

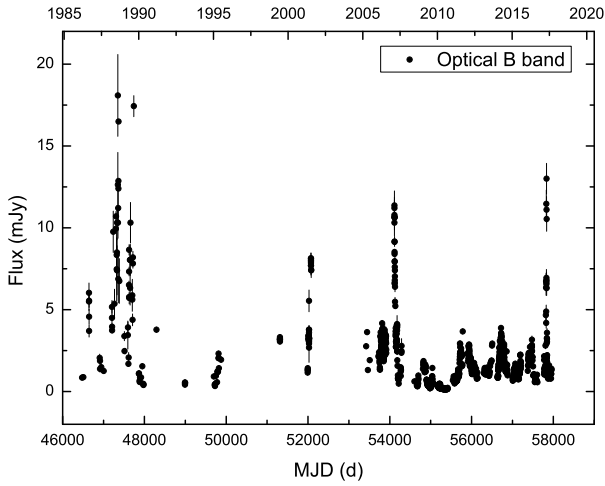


Fig. 2 The long-term optical B band light curve of blazar 3C 279. Calendar dates are along the top and MJDs are expressed at the bottom.

2 LIGHT CURVES

2.1 Optical Band

We have compiled the observed data in the optical R band from different literatures (Chatterjee et al. 2008; Dai et al. 2001; Ghosh et al. 2000; Grandi et al. 1996; Hartman et al. 1996; Hayashida et al. 2012; Kartaltepe & Balonek 2007; Katajainen et al. 2000; Kidger et al. 1992a; Kiehlmann et al. 2016; Larionov et al. 2008; Mead et al. 1990; Nilsson et al. 2018; Sandrinelli et al. 2016; Shrader et al. 1994; Takalo et al. 1992; Villata et al. 1997; Webb et al. 1990; Xie et al. 1999, 2001, 2002) and some groups, such as the Small and Moderate Aperture Research Telescope System (SMARTS) (Bonning et al. 2012), the Steward Observatory monitoring project (Smith et al. 2009) and the 0.76-m Katzman Automatic Imaging Telescope (Li et al. 2003). Totally, there are 7299 data points in the optical R band light curve. The length of the data series is over a span of 32 yr, from Modified Julian Date (MJD) 46646 to 58306. The light curve has been presented in panel (a) of Figure 1. The figure confirms that the source exhibits some large outbursts near MJD 52126, 54113 and 57834. There is also a huge outburst with $F_R = 121.5$ mJy ($R = 11.01$ mag) on 47306. Due to the scale, it is not included in the figure. Additionally, there are still some slightly smaller flares. It seems that the source bursts more frequently before MJD 52000 than after. During the past three decades, the source has varied violently with $\Delta R = 7.08$ mag. Meanwhile, we have collected data from the optical B band, which consist of 1083 points (see Fig. 2). Webb et al. (1990) observed a big outburst in 1988 with $B = 12.13$ mag. Nevertheless, it was still 0.83 mag fainter than the one during 1936–1937 ($B = 11.3$ mag).

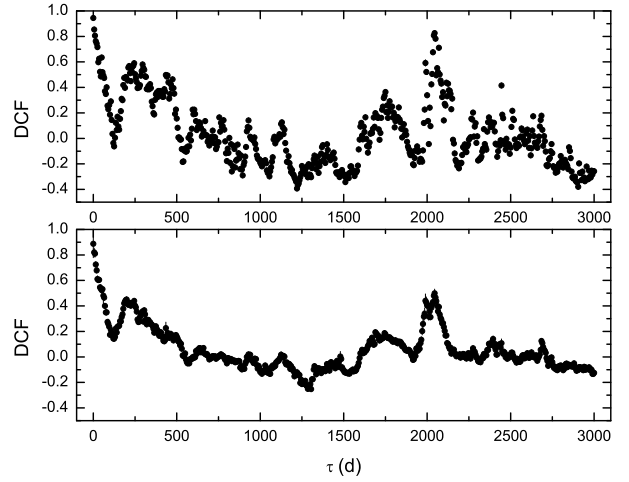


Fig. 3 The auto-DCF of the optical R band light curve of 3C 279. The *upper panel* is the auto-DCF for the full light curve, and the *lower panel* is the auto-DCF for a one-day averaged light curve.

2.2 RXTE X-ray

The *Rossi X-ray Timing Explorer (RXTE)* acquired sustained long-term X-ray observations of sources during its mission from December 1995 to January 2012, and it provided 2–10 keV light curves from the Proportional Counter Array (PCA) data with one point per observation (Rivers et al. 2013). 3C 279 was continually monitored with 2–3 points per week from MJD 50104 (1996 January 22) to 55925 (2011 December 30), and the total good exposure time of PCA is 2222 ks. The light curve includes 1987 observations and data points with a time coverage of about 15 yr¹. It is plotted in panel (b) of Figure 1. One can see that it exhibits four main outbursts in the light curve as well as some low amplitude flares.

2.3 Swift X-ray

3C 279 was observed by the X-ray Telescope (XRT) equipped on the satellite *Swift* from MJD 53748 to 58299 with 6.89×10^5 s of exposure time, which spans about 12.5 yr. The data set is comprised of 471 points². The analysis methods utilized to produce X-ray light curves were described by Stroh & Falcone (2013). The light curve is displayed in panel (c) of Figure 1. One can see that 3C 279 exhibits the largest outburst on MJD 58135 (2018 January 17) since it was observed in January 2006. Then, 143 d after this outburst, a following one appeared on MJD 58278 (2018 June 9). Another outburst can be seen on MJD 57189 (2015 June 6). In addition, there are some flares in the light curve accompanied by some gaps.

¹ <https://cass.ucsd.edu/~rxteagn/>

² <https://www.swift.psu.edu/monitoring>

2.4 Fermi γ -ray

Fermi-LAT is a γ -ray telescope which is sensitive to the energy of 20 MeV – 300 GeV (Atwood et al. 2009). *Fermi* covers the entire sky every 90 min. 3C 279 was observed from MJD 54691 (2008 August 13) to 58893 (2020 February 14) with a time span of about 11.5 yr. Its daily flux was provided by *Fermi*-LAT³. The light curve is comprised of 130 data points and is drawn in panel (d) of Figure 1. From the light curve, one can see an obvious outburst on MJD 57189 (2015 June 6). During the outburst, the flux increased by 12.5 times in 5 d, then decreased by 97.3% in 5 d. There are two other large outbursts on MJD 58136 (2018 January 18) and 58228 (2018 April 20), respectively. This means that 3C 279 is a highly variable source in the γ -ray band.

3 PERIODICITY

3.1 DCF Method

The discrete correlation function (DCF) method was presented by Edelson & Krolik (1988) to search for correlations and possible time delays between two different data sets. The method can also be used to search for a possible periodic component in a single light curve. This method takes full advantage of all available data points, and no interpolation is required in the light curve. So, it is peculiarly propitious for unevenly sampled variability data. Given a time delay τ , all data pairs with time delay of $\Delta t_{ij} \in [\tau - \Delta\tau/2, \tau + \Delta\tau/2)$ are employed to compute the DCF $_{\tau}$

$$\text{DCF}(\tau) = \frac{\langle (a_i - \bar{a})(b_j - \bar{b}) \rangle}{\sigma_a \sigma_b} \quad (1)$$

for two light curves a and b , where a_i and b_j are the fluxes of data points, \bar{a} and \bar{b} are the flux means, and σ_a and σ_b are the standard deviations, respectively (White & Peterson 1994; Fuhrmann et al. 2014).

For each time delay, τ , there is a DCF corresponding to it. The DCF peak means two light curves are correlated with each other, and a delay of τ exists. For a single light curve, the evident peak of auto-DCF indicates the existence of periodic signals. In general, the Monte Carlo simulation method is applied to evaluate the time delay and its error (Peterson et al. 1998; Raiteri et al. 2003).

3.2 Periodicity Analysis

The long-term optical R band light curve of 3C 279 is searched by the DCF method to find possible periodic or quasi-periodic signals. The DCF result is plotted in

³ https://fermi.gsfc.nasa.gov/ssc/data/access/lat/ms1_lc/

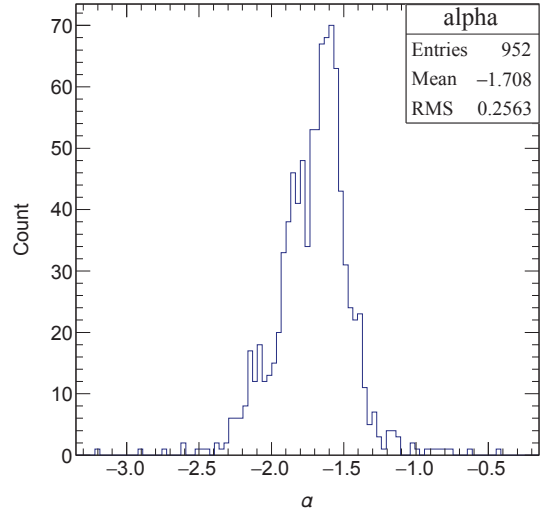


Fig. 4 The distribution of optical spectral indices α .

Figure 3. Besides a peak at zero, there exists an obvious peak at 2045 d with DCF = 0.83 ± 0.01 . Five-thousand simulations have been performed, and the peak position as well as its uncertainties is derived to be 2044 ± 2.1 d. To suppress spurious signals, the light curve is averaged daily. The corresponding DCF is also plotted in Figure 3. The peak is still at $\tau = 2045$ d, but much lower, which equals 0.50 ± 0.03 . Light curve simulations show that its significance is 4.1σ . This means the light curve has a very weak 5.6-yr quasi-periodic variation component.

From the light curve, one can see several obvious outbursts. The result of $\tau = 5.6$ yr may be dominated by some outburst pairs, which have about 5.6-yr-long intervals, such as, the outbursts on MJD 57834 and 55719 with an interval of 5.79 yr, the outbursts on MJD 55719 and 54113 with an interval of 4.4 yr, the outbursts on MJD 54113 and 52126 with an interval of 5.44 yr, the pairs on MJD 52126 and 50136 with an interval of 5.45 yr, and the pairs on MJD 50936 and 48789 with an interval of 5.88 yr. It should be noted that there is a huge outburst on MJD 47306 without a counterpart.

4 SPECTRAL BEHAVIOR INVESTIGATION

The spectrum generally follows a power law for blazars, which is,

$$F \propto \nu^\alpha, \quad (2)$$

where F represents the flux, ν corresponds to the frequency and α signifies the spectral index.

Then the spectral index can be computed as

$$\alpha = \frac{\log F_2 - \log F_1}{\log \nu_2 - \log \nu_1} \quad (3)$$

where subscripts 1 and 2 denote two different observation bands.

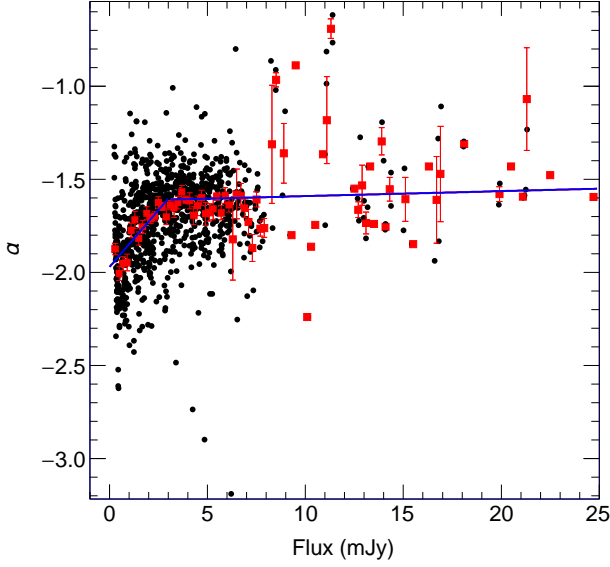


Fig. 5 Optical spectral index versus R band flux. The red squares with error bars represent the average values of α_s . The two blue lines indicate the linear fitting results.

The optical variations are always accompanied by spectral variations. To investigate the spectral behavior, we have computed the optical spectral index between optical B and R bands. Quasi-simultaneous $B - R$ pairs of observations with intervals less than 30 min are chosen for the analysis. In addition, a correction for interstellar extinction is introduced. For 3C 279, the color excess due to interstellar extinction is $E_{B-V} = 0.03^m$ (Mead et al. 1990), and then the interstellar extinction A_V in the V band is 0.093^m . Using the normal interstellar extinction curve (Schlegel et al. 1998), we obtain B and R band extinctions. The values of A_B and A_R are 0.123^m and 0.078^m , respectively. After correction, the α_s are calculated with Equation (3). The distribution of α_s is given in Figure 4, which indicates the α_s have a mean value of -1.71 ± 0.26 .

The change of spectral index with flux is presented by black dots in Figure 5. One can see that these points are very scattered. However, they have a gradual rising trend from the overall outline, which means the spectrum becomes flatter as the flux increases. However, if we examine the details, there seem to be a fine structure. To see clearly, we calculate the average values of α_s at different fluxes, and superimpose them on Figure 5 with red squares and error bars. An obvious variation tendency can be clearly ascertained. The spectral index increases from -2.0 to -1.6 with the brightness increasing, and then hardly increases any more when flux reaches a certain value around 3 mJy (15.03 mag).

The data are divided into two segments and fitted with two different linear functions. The fitted results are also superimposed on Figure 5 with two blue lines. When fluxes

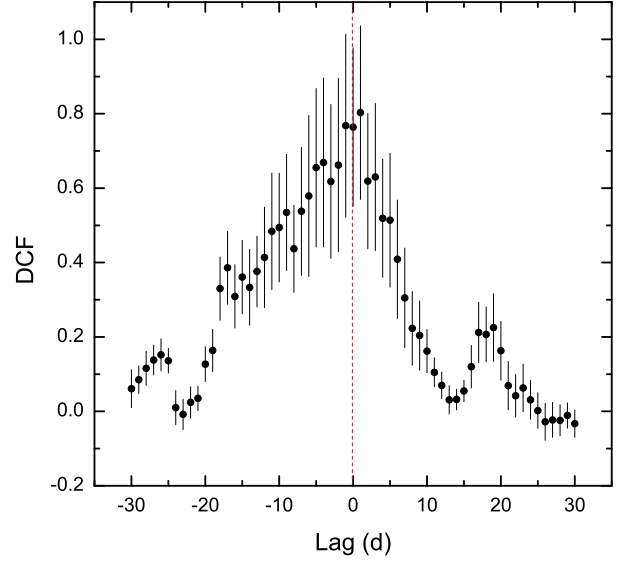


Fig. 6 The DCF between *Fermi* γ -ray and *Swift* X-ray bands of 3C 279. The red vertical dashed line highlights the position of zero.

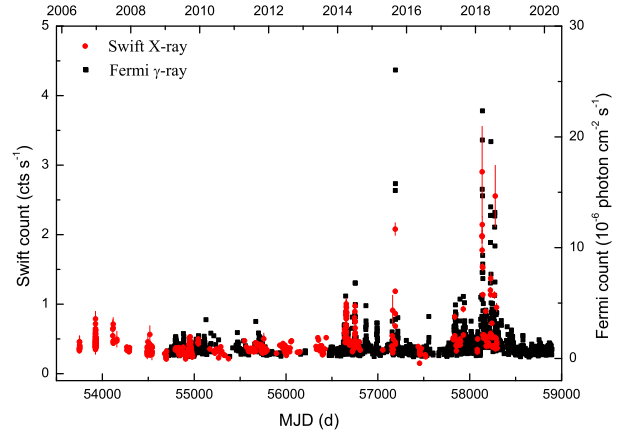


Fig. 7 The light curves of *Fermi* γ -ray (black squares) and *Swift* X-ray (red dots) bands.

of R band, F_R , are below 3 mJy,

$$\alpha = (0.123 \pm 0.011)F_R - (1.970 \pm 0.020), \quad (4)$$

and when above 3 mJy,

$$\alpha = (0.003 \pm 0.001)F_R - (1.617 \pm 0.009). \quad (5)$$

The fitting results indicate that in the low state of the source, α increases obviously with the increase of brightness, and then stays roughly stable in the high state.

5 CORRELATION ANALYSIS

5.1 Correlation between γ -ray and X-ray Bands

The light curves of γ -ray and X-ray (observed by *Swift*-XRT) have about 9.9 yr of overlap from MJD 54691 to

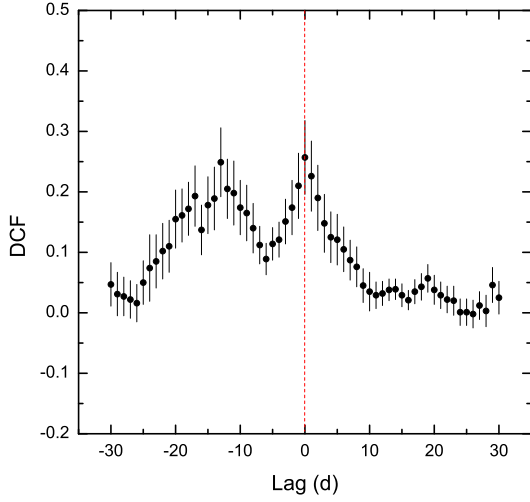


Fig. 8 The DCF between *Fermi* γ -ray and optical *R* bands. The red vertical dashed line highlights the position of zero.

58299 (see panels (d) and (c) in Fig. 1). We apply the DCF method to analyze the relation between the two light curves with $\Delta\tau = 1$ d. An obvious peak (DCF = 0.80 ± 0.23) is visible at $\tau = 1$ d (Fig. 6). We have performed 5000 Monte Carlo simulations, and derived $\tau_{center} = 0.0^{+1.0}_{-1.8}$ d and DCF = $0.85^{+0.05}_{-0.06}$, which implies that γ -ray variations are correlated well with X-ray ones without time lags. To clearly view the variation trends, we have plotted these two light curves on the same panel in Figure 7. The light curves have similar structures and trends, and they vary synchronously (in step), especially during the main outbursts during June 2015, January 2018 and April 2018.

5.2 Correlation between γ -ray and Optical Bands

Light curves of γ -ray and optical *R* bands have a 10.8-yr-long overlap from MJD 54691 to 58637 (see panels (d) and (a) in Fig. 1). The correlation between them is investigated by the DCF method. Figure 8 presents the result, which has a peak of 0.26 ± 0.06 at zero as well as another peak of 0.25 ± 0.06 at -13 d. Using 5000 simulations, we have derived τ_{center} to be $-0.5^{+1.0}_{-12.5}$ d, and DCF to be $0.31^{+0.05}_{-0.05}$. This suggests that variations in the γ -ray band are weakly correlated with those of optical bands. From panels (a) and (d) in Figure 1, one can see that almost each flare in the γ -ray band has a counterpart in the optical band. Two light curves are superimposed on each other, and are plotted in Figure 9 to exhibit the details of variations. One can see that the corresponding scintillation of two light curves occurs at almost the same time (simultaneously), but the amplitude of variations is not very proportional. For example, in the light curve of the optical band, the burst on MJD 57834 is greater than that on MJD 58271. In the γ -ray region, however, the opposite is true.

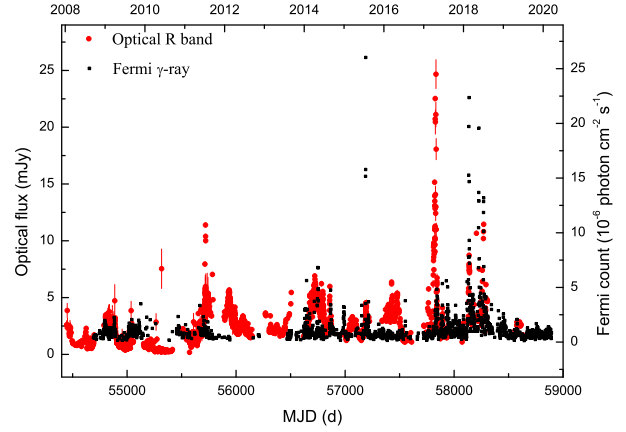


Fig. 9 The light curves of *Fermi* γ -ray (black squares) and optical *R* (red dots) bands.

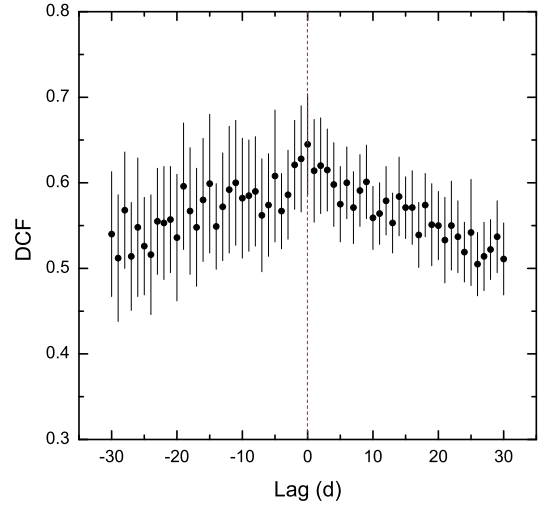


Fig. 10 The DCF between *RXTE* X-ray and optical *R* bands. The red vertical dashed line is drawn to guide the eyes.

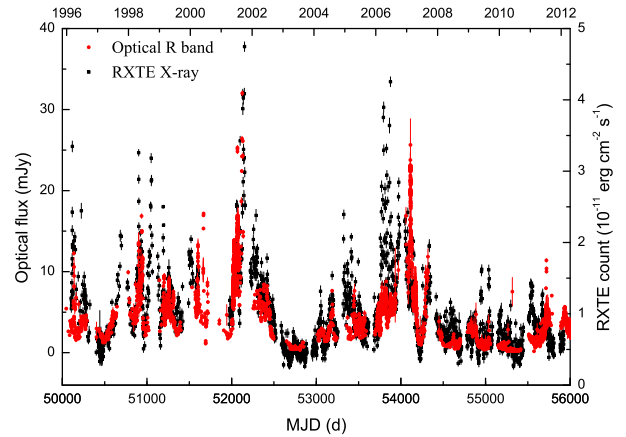


Fig. 11 The light curves of *RXTE* X-ray (black squares) and optical (red dots) bands. Only a partial optical light curve has been plotted.

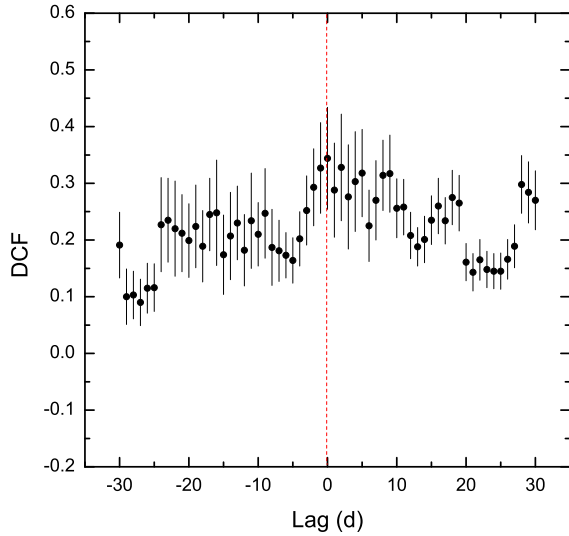


Fig. 12 The DCF between *Swift* X-ray and optical *R* bands. The vertical red dashed line is for guiding the eyes.

5.3 Correlation between X-ray and Optical Bands

The results of DCF, between X-ray (observed by *RXTE*-PCA) and optical *R* light curves, are presented in Figure 10. There is an obvious peak ($\text{DCF} = 0.65 \pm 0.06$) at zero. To estimate the error of time delay, we have performed 5000 simulations, and obtained $\tau_{\text{center}} = 0.0_{-4.4}^{+4.8}$ d with $\text{DCF} = 0.67_{-0.03}^{+0.03}$. This means that the light curve of X-ray band correlates well with that of the optical band with zero lag. In light curves plotted in Figure 1, we have drawn some vertical red dotted lines near the peaks to guide the eyes. The two light curves exhibit flares simultaneously. Four main peaks (near MJD 54113, 52126, 50936 and 50136) in the light curve of the optical band all have counterparts in the *RXTE* X-ray light curve. However, the X-ray flare in early 2006 seems to have no optical counterpart. To see details of variations, we have superimposed the light curve from the optical band on that of the *RXTE* X-ray band, and display them in the same panel (Fig. 11). It is quite apparent that the variation trends are very similar to each other.

There is a 12.5-yr overlap between *Swift* X-ray and optical light curves from MJD 53748 to 58299. We have also investigated the correlation between two light curves. The DCF result is given in Figure 12. There is a peak with $\text{DCF} = 0.34 \pm 0.09$ at $\tau = 0$ d. According to 5000 simulations, the mean value of time delay is derived to be $1.9_{-3.5}^{+7.0}$ d, and $\text{DCF} = 0.43_{-0.05}^{+0.06}$. The two curves are superimposed on each other, which have been shown in Figure 13. The source bursts almost simultaneously, and the light curves have similar trends. However, the magnitudes of the main flares are disproportionate. For example, around MJD 57837, the X-ray burst looks lower

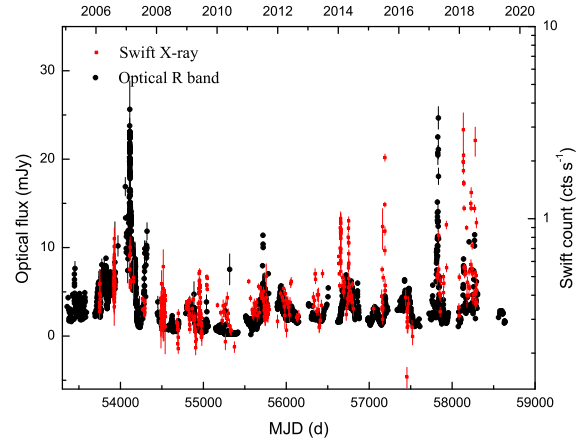


Fig. 13 The light curves of *Swift* X-ray (red squares) and optical (black dots) bands.

than its counterpart in the optical band, whereas around MJD 57189 and 58135 they are opposite. This may be one reason that results in the low DCF peak.

The two X-ray light curves observed by *RXTE* and *Swift* have also been analyzed by means of the DCF method. The result, $\text{DCF}(-1.5_{-1.9}^{+1.9}) = 0.82_{-0.04}^{+0.04}$, signifies that they are well correlated with each other.

6 DISCUSSION AND CONCLUSIONS

6.1 Periodicity

In the 32-yr-long optical *R* band light curve, we found that a possible 2044-d (5.6-yr) quasi-periodic variation component exists. The outbursts appear periodically with approximately 5.6-yr intervals (5.79 yr, 4.40 yr, 5.44 yr, 5.45 yr and 5.88 yr). However, the variation is complex. There are some smaller outbursts in the light curve. The 10-d-averaged light curve has also been adopted to search for a periodic component. The DCF peak is located on $\tau = 5.5$ yr, although the value of DCF drops down to 0.38. This suggests the source varies with a weak quasi-periodicity of ~ 5.6 yr. Thus it can be predicted that the next outburst may happen in October-November 2022 corresponding to the outburst during March 2017.

On a medium timescale, Li et al. (2009) detected a 130.6-d outburst periodicity. However, with ten years of photometric data from September 2002 to September 2012, Nilsson et al. (2018) found no significant periodicity in the optical light curve of 3C 279. Examining optical data between 1929 and 1952, Eachus & Liller (1975) inferred that a tendency exists to repeat outbursts at ~ 7 yr intervals. We have re-examined that light curve. During 1936-1937, there is a double maximum structure with $B \sim 12.10^m$ and $B \sim 11.27^m$ located on MJD ~ 28305 and ~ 28635 , respectively, which is separated by an interval of 330 d (0.9 yr). After this, on MJD ~ 30843 , there is another maximum

with $B \sim 13.29^m$. According to two separated bursts, there is an interval of ~ 6 yr.

Periodic signals have been derived in several sources. For example, an 11–12 yr periodicity for OJ 287 has been detected by Sillanpaa et al. (1988) and Kidger et al. (1992b). A 317-d periodicity for PKS 2155–304 has been claimed by Zhang et al. (2014), and then confirmed by Sandrinelli et al. (2014). Evidence of quasi-periods of ~ 3 and ~ 1.9 yrs has been found for 3C 66A and B2 1633+38, respectively (Otero-Santos et al. 2020). The phenomenon of quasi-periodicities has been interpreted by several different models. The supermassive binary black hole (SMBBH) model has been proposed to interpret quasi-periodic variations. The secondary black hole may change the accretion rate, or lead to jet precession, then, the precession causes variation in the Doppler factor. Helical structured jets also cause changes in the Doppler factor. There are other mechanisms such as recurrent shock front formation or disk instability, which could produce quasi-periodical variability in the light curve (see Sandrinelli et al. 2018; Otero-Santos et al. 2020; Yang et al. 2020; Agarwal et al. 2021, and references therein).

6.2 Spectral Index

The variability in brightness is usually accompanied by that in spectral index. On long timescales, the source 3C 279 displays a complicated optical spectral behavior. In this analysis, the source exhibits considerable variation in optical spectral index and has a mean value of -1.71 . Webb et al. (1990) reported a spectral index variation range of $-2.05 \sim -0.55$ for 3C 279 with an average of -1.12 . Some other reports stated that the optical spectral index of 3C 279 varied from -2.17 to -0.6 (O’Dell et al. 1978; Sitko et al. 1982; Brown et al. 1989; Netzer et al. 1996; Grandi et al. 1996).

The optical spectral behavior has been explored for a number of blazars (see Rani et al. 2010; Zhang et al. 2015; Raiteri et al. 2017, and references therein). In general, there are two typical spectral behaviors. One case is when the brightness increases, the source turns blue (i.e., the spectrum becomes flat). In another case, just the opposite, the source turns red when the brightness increases (i.e., the spectrum becomes steep). In addition, there are some complex spectral behaviors. For several blazars, when they are in low states, the energy spectra become steeper as the brightness increases. However, when they are in high states, the spectra become flatter or remain unchanged as the brightness increases (Villata et al. 2006; Ikejiri et al. 2011; Zhang et al. 2013, 2015; Isler et al. 2017). For 3C 279, the short-term color variations have

been studied, which has been found to show, in some cases, no apparent correlation between spectral index and brightness (Brown et al. 1989; Webb et al. 1990), and in other cases the source exhibits a clear bluer trend when the brightness increases (Shrader et al. 1994; Larionov et al. 2008; Rani et al. 2010; Zhang et al. 2015). With over 7 yr of SMARTS monitoring, Isler et al. (2017) ascertained the optical/near-infrared (OIR) color of 3C 279 was averagely bluer when brighter. However, on shorter timescales, the source exhibited different color behaviors, such as bluer when brighter, redder when brighter and achromatic phenomenon. In this analysis, although the dots in the diagram of α –Flux are very scattered on a long-timescale, the profile (average trend) exhibits an obvious relation between spectral index and flux (see Fig. 5). When the R band flux is less than 3 mJy (15.03 mag), 3C 279 becomes blue as brightness increases. If we zoom in on the figure, we can see that, in the lowest state (Flux $\leq \sim 0.5$ mJy), the source becomes blue as brightness decreases. These results are in agreement with those presented by Isler et al. (2017). However, in the case of the source being brighter than 3 mJy, it remains stable (stable-when-brighter) with a mean value of $\alpha \simeq -1.6$. These phenomena may be explained by a combination and different contributions of non-thermal jet and thermal accretion disk emission. Redder-when-brighter is due to a faint jet emission and a strong blue disk emission (Villata et al. 2006; Ikejiri et al. 2011; Isler et al. 2017). A variable source with constant and bluer color and an underlying redder source in the jet may cause the bluer-when-brighter phenomenon (Ikejiri et al. 2011). When the jet becomes progressively brighter, the variable component will be much greater than the underlying component, and then the color tends to stabilize.

6.3 Correlation

In this analysis, 3C 279 manifests violent variabilities in all three bands of γ -ray, X-ray and optical R bands. Almost each main outburst in one light curve has corresponding outbursts in the others.

During January–February 1996, an X-ray outburst (*RXTE*) of 3C 279 showed a good correlation with the γ -ray flare with no lags (Wehrle et al. 1998). However, Hayashida et al. (2012) indicated that there was no correlation between the variations of X-ray and γ -ray bands during 2008–2010. Fraija et al. (2019) investigated the correlation between γ -ray and X-ray, and derived a low DCF (~ 0.05) peak close to zero lag during the flare from February–April 2014 (MJD 56695–56775). Recently, Larionov et al. (2020) found the variations of X-ray and γ -ray bands were well correlated with each other. On a long timescale, we find the variations are well correlated

Table 1 Correlation Analysis between Individual Main Outbursts of γ -ray, X-ray and Optical Bands.

Outburst	DCF	τ (d)	Bands
MJD 58200–58400	0.66 ± 0.28	0	γ -ray vs. X-ray
MJD 58000–58200	0.92 ± 0.27	0	γ -ray vs. X-ray
MJD 56900–57300	0.98 ± 0.73	-1	γ -ray vs. X-ray
MJD 56300–56900	0.43 ± 0.15^a	0	γ -ray vs. X-ray
MJD 58200–58400	0.91 ± 0.40	0	γ -ray vs. Optical
MJD 58000–58200	0.92 ± 0.32	0	γ -ray vs. Optical
MJD 57840–58000	0.79 ± 0.23	0	γ -ray vs. Optical
MJD 57700–57840	0.89 ± 0.26	0	γ -ray vs. Optical
MJD 56900–57300	0.50 ± 0.31^b	0	γ -ray vs. Optical
MJD 58200–58400	0.94 ± 0.55	0	X-ray vs. Optical
MJD 58000–58200	0.96 ± 0.18	2	X-ray vs. Optical
MJD 57700–58000	0.96 ± 0.69	-2	X-ray vs. Optical
MJD 56900–57300	0.83 ± 0.42^c	1	X-ray vs. Optical

^a There is another peak, $DCF(10) = 0.46 \pm 0.20$; ^b There is another peak, $DCF(7) = 0.59 \pm 0.34$; ^c There is another peak, $DCF(7) = 0.97 \pm 0.88$.

between γ -ray and X-ray with no delay in this analysis. Individual outbursts have also been investigated by the DCF method, and they show good correlations with each other (see Table 1). The simultaneous correlated variability in γ -ray and X-ray indicates they are approximately co-spatial (Wehrle et al. 1998). 3C 279 is a low-frequency peaked blazar. The radiation of radio to ultraviolet (UV) wavelengths is generated through the synchrotron process by relativistic electrons in the jet, and X-rays and γ -rays are produced by scattering soft-target photons in or out of the jet. The X-rays and γ -rays might be the low and high energy ends of the same inverse-Compton emission component, respectively (Hayashida et al. 2015).

With data from 2008–2010, Hayashida et al. (2012) reported a possible 10-d delay between the optical and γ -ray emissions. However, Janiak et al. (2012) emphasized that a 10-d lag is just a possibility as the result may be misled by poor data quality. Fraija et al. (2019) also suggested no correlation between γ -ray and optical bands during 2008–2010 since the peak of $DCF = \sim 0.055$ at the lag of 31 d. Larionov et al. (2020) suggested that the correlation was rather weak between γ -ray and optical bands, and the relation changed with activity state. In this analysis, the variations of γ -ray and optical R bands exhibit a weak correlation. The low DCF may be due to the disproportion between different outbursts. We thus investigate the individual γ -ray outbursts. For the outburst during MJD 58200–58400 (March - October 2018), $DCF(0) = 0.91 \pm 0.40$. The DCF results from the individual main outbursts are listed in Table 1, which indicate that the variations in γ -ray have strong correlations with those in the optical band, and there are no obvious time delays. There is evidence to support that optical and γ -ray emission regions have common spatiality (Abdo et al. 2010). In the simplest case, the connection between the flares of optical and gamma-ray bands can be predicted by both synchrotron self-Compton (SSC)

and external Compton (EC) models (Reinthal et al. 2012). Cohen et al. (2014) found clear correlations between optical and γ -ray variations in 30 out of the 40 brightest blazars, which clearly favored the leptonic model used to explain blazar radiation.

Larionov et al. (2008) pointed out the X-ray–optical correlation of 3C 279 was rather weak during 2006–2007, with variations in X-ray being ~ 1 d ahead of optical (R) variations. Chatterjee et al. (2008) also identified significant correlations between the variations of X-ray (observed by *RXTE*) and optical R bands during 1996–2007. Fraija et al. (2019) indicated no correlation between X-ray and optical bands during 2009. In this analysis, for X-ray (observed by *RXTE*) and optical R bands, their variation trends are very similar. They exhibit strong correlation with each other. However, DCF results have revealed that X-ray (observed by *Swift*) variations are weakly correlated with those of the optical band. If we examine the light curves in detail (Fig. 13), we find the source bursts almost simultaneously, and the light curves have similar trends. However, the magnitude of the main flares is not proportionate. We have checked individual bursts in X-ray band. For the maximal outburst of X-ray on MJD 58000–58200 (September 2017 to March 2018), DCF of X-ray and optical bands equals 0.96 at 2 d. The DCF results of other bursts have been investigated and are listed in Table 1. For each outburst of X-ray and optical bands, the variations are well correlated. This indicates that the optical flares are emitted by the synchrotron process, and the X-ray emission is not simply an extension of the synchrotron process, but instead, includes the contribution of inverse Compton scattering components of low energy electrons (Larionov et al. 2008; Chatterjee et al. 2008; Abdo et al. 2010; Chatterjee et al. 2012).

To conclude, we have compiled the long term optical, X-ray and γ -ray light curves of blazar 3C 279. The source

exhibits violent variabilities in all those three bands. In the optical band, 3C 279 has been found to display a possible 5.6-yr-long weak quasi-periodic variation component, that exhibits different spectral behaviors in different states, with a clear flatter-when-brighter trend in low states and a stable-when-brighter trend in high states. The correlation analysis concludes that γ -ray and X-ray variations are strongly correlated with each other, but weakly with those of optical R band. However, in the course of the main outbursts, the variations of γ -ray, X-ray and optical R bands manifest strong correlations with each other and with no obvious time lag. The results imply that the optical emissions are produced by the synchrotron process, and the X-ray and γ -ray emissions by inverse Compton scattering, and their emission regions are approximately co-spatial.

Acknowledgements We thank the support from National Natural Science Foundation of China (NSFC, Nos. U1831124 and 11273008), and the Natural Science Foundation of Anhui Province of China (Grant No. 1908085MA28). We also thank the WEBT groups for providing their optical data.

References

- Abdo, A. A., Ackermann, M., Ajello, M., et al. 2010, *Nature*, 463, 919
- Agarwal, A., Mihov, B., Andruchow, I., et al. 2021, *A&A*, 645, A137
- Aleksić, J., Ansoldi, S., Antonelli, L. A., et al. 2014, *A&A*, 567, A41
- Atwood, W. B., Abdo, A. A., Ackermann, M., et al. 2009, *ApJ*, 697, 1071
- Bonning, E., Urry, C. M., Bailyn, C., et al. 2012, *ApJ*, 756, 13
- Böttcher, M., Basu, S., Joshi, M., et al. 2007, *ApJ*, 670, 968
- Brown, L. M. J., Robson, E. I., Gear, W. K., et al. 1989, *ApJ*, 340, 129
- Chatterjee, R., Jorstad, S. G., Marscher, A. P., et al. 2008, *ApJ*, 689, 79
- Chatterjee, R., Bailyn, C. D., Bonning, E. W., et al. 2012, *ApJ*, 749, 191
- Cohen, D. P., Romani, R. W., Filippenko, A. V., et al. 2014, *ApJ*, 797, 137
- Dai, B. Z., Xie, G. Z., Li, K. H., et al. 2001, *AJ*, 122, 2901
- Eachus, L. J., & Liller, W. 1975, *ApJL*, 200, L61
- Edelson, R. A., & Krolik, J. H. 1988, *ApJ*, 333, 646
- Fan, J. H. 1999, *MNRAS*, 308, 1032
- Frajia, N., Benítez, E., Hiriart, D., et al. 2019, *ApJS*, 245, 18
- Fuhrmann, L., Larsson, S., Chiang, J., et al. 2014, *MNRAS*, 441, 1899
- Ghosh, K. K., Ramsey, B. D., Sadun, A. C., & Soundararajaperumal, S. 2000, *ApJS*, 127, 11
- Grandi, P., Urry, C. M., Maraschi, L., et al. 1996, *ApJ*, 459, 73
- Hartman, R. C., Bertsch, D. L., Fichtel, C. E., et al. 1992, *ApJL*, 385, L1
- Hartman, R. C., Webb, J. R., Marscher, A. P., et al. 1996, *ApJ*, 461, 698
- Hartman, R. C., Villata, M., Balonek, T. J., et al. 2001, *ApJ*, 558, 583
- Hayashida, M., Madejski, G. M., Nalewajko, K., et al. 2012, *ApJ*, 754, 114
- Hayashida, M., Nalewajko, K., Madejski, G. M., et al. 2015, *ApJ*, 807, 79
- Ikejiri, Y., Uemura, M., Sasada, M., et al. 2011, *PASJ*, 63, 639
- Isler, J. C., Urry, C. M., Coppi, P., et al. 2017, *ApJ*, 844, 107
- Janiak, M., Sikora, M., Nalewajko, K., Moderski, R., & Madejski, G. M. 2012, *ApJ*, 760, 129
- Jorstad, S. G., Marscher, A. P., Lister, M. L., et al. 2004, *AJ*, 127, 3115
- Kartalpe, J. S., & Balonek, T. J. 2007, *AJ*, 133, 2866
- Katajainen, S., Takalo, L. O., Sillanpää, A., et al. 2000, *A&AS*, 143, 357
- Kidger, M., Lario, P. G., & de Diego, J. A. 1992a, *A&AS*, 93, 391
- Kidger, M., Takalo, L., & Sillanpää, A. 1992b, *A&A*, 264, 32
- Kiehlmann, S., Savolainen, T., Jorstad, S. G., et al. 2016, *A&A*, 590, A10
- Larionov, V. M., Jorstad, S. G., Marscher, A. P., et al. 2008, *A&A*, 492, 389
- Larionov, V. M., Jorstad, S. G., Marscher, A. P., et al. 2020, *MNRAS*, 492, 3829
- Li, H. Z., Xie, G. Z., Chen, L. E., et al. 2009, *PASP*, 121, 1172
- Li, W., Filippenko, A. V., Chornock, R., & Jha, S. 2003, *PASP*, 115, 844
- MAGIC Collaboration, Albert, J., Aliu, E., et al. 2008, *Science*, 320, 1752
- Mead, A. R. G., Ballard, K. R., Brand, P. W. J. L., et al. 1990, *A&AS*, 83, 183
- Netzer, H., Heller, A., Loinger, F., et al. 1996, *MNRAS*, 279, 429
- Nilsson, K., Lindfors, E., Takalo, L. O., et al. 2018, *A&A*, 620, A185
- O’Dell, S. L., Puschell, J. J., Stein, W. A., & Warner, J. W. 1978, *ApJS*, 38, 267
- Otero-Santos, J., Acosta-Pulido, J. A., Becerra González, J., et al. 2020, *MNRAS*, 492, 5524
- Paliya, V. S., Sahayanathan, S., & Stalin, C. S. 2015, *ApJ*, 803, 15
- Peterson, B. M., Wanders, I., Horne, K., et al. 1998, *PASP*, 110, 660
- Prince, R. 2020, *ApJ*, 890, 164
- Raiteri, C. M., Villata, M., Tosti, G., et al. 2003, *A&A*, 402, 151
- Raiteri, C. M., Villata, M., Acosta-Pulido, J. A., et al. 2017, *Nature*, 552, 374
- Rani, B., Gupta, A. C., Strigachev, A., et al. 2010, *MNRAS*, 404, 1992
- Reinthal, R., Lindfors, E. J., Mazin, D., et al. 2012, in

- Journal of Physics Conference Series, 355, Journal of Physics Conference Series, 012013
- Rivers, E., Markowitz, A., & Rothschild, R. 2013, *ApJ*, 772, 114
- Sandrinelli, A., Covino, S., & Treves, A. 2014, *ApJL*, 793, L1
- Sandrinelli, A., Covino, S., Dotti, M., & Treves, A. 2016, *AJ*, 151, 54
- Sandrinelli, A., Covino, S., Treves, A., et al. 2018, *A&A*, 615, A118
- Schlegel, D. J., Finkbeiner, D. P., & Davis, M. 1998, *ApJ*, 500, 525
- Shah, Z., Jithesh, V., Sahayanathan, S., Misra, R., & Iqbal, N. 2019, *MNRAS*, 484, 3168
- Shrader, C. R., Webb, J. R., Balonek, T. J., et al. 1994, *AJ*, 107, 904
- Sillanpaa, A., Haarala, S., Valtonen, M. J., Sundelius, B., & Byrd, G. G. 1988, *ApJ*, 325, 628
- Sitko, M. L., Stein, W. A., Zhang, Y. X., & Wisniewski, W. Z. 1982, *ApJ*, 259, 486
- Smith, P. S., Montiel, E., Rightley, S., et al. 2009, arXiv e-prints, arXiv:0912.3621
- Stroh, M. C., & Falcone, A. D. 2013, *ApJS*, 207, 28
- Takalo, L. O., Sillanpaa, A., Nilsson, K., et al. 1992, *A&AS*, 94, 37
- Tornikoski, M., Valtaoja, E., Terasranta, H., et al. 1994, *A&A*, 289, 673
- Unwin, S. C., Cohen, M. H., Biretta, J. A., Hodges, M. W., & Zensus, J. A. 1989, *ApJ*, 340, 117
- Urry, C. M., & Padovani, P. 1995, *PASP*, 107, 803
- Villata, M., Raiteri, C. M., Ghisellini, G., et al. 1997, *A&AS*, 121, 119
- Villata, M., Raiteri, C. M., Balonek, T. J., et al. 2006, *A&A*, 453, 817
- Webb, J. R., Carini, M. T., Clements, S., et al. 1990, *AJ*, 100, 1452
- Wehrle, A. E., Pian, E., Urry, C. M., et al. 1998, *ApJ*, 497, 178
- White, R. J., & Peterson, B. M. 1994, *PASP*, 106, 879
- Whitney, A. R., Shapiro, I. I., Rogers, A. E. E., et al. 1971, *Science*, 173, 225
- Xie, G. Z., Li, K. H., Bai, J. M., et al. 2001, *ApJ*, 548, 200
- Xie, G. Z., Li, K. H., Zhang, X., Bai, J. M., & Liu, W. W. 1999, *ApJ*, 522, 846
- Xie, G. Z., Liang, E. W., Zhou, S. B., et al. 2002, *MNRAS*, 334, 459
- Yang, X., Yi, T., Zhang, Y., et al. 2020, *PASP*, 132, 044101
- Zhang, B.-K., Wang, S., Zhao, X.-Y., Dai, B.-Z., & Zha, M. 2013, *MNRAS*, 428, 3630
- Zhang, B.-K., Zhao, X.-Y., Wang, C.-X., & Dai, B.-Z. 2014, *RAA (Research in Astronomy and Astrophysics)*, 14, 933
- Zhang, B. K., Zhao, X. Y., Zhang, L., & Dai, B. Z. 2017, *ApJS*, 231, 14
- Zhang, B.-K., Zhou, X.-S., Zhao, X.-Y., & Dai, B.-Z. 2015, *RAA (Research in Astronomy and Astrophysics)*, 15, 1784